



**HAL**  
open science

# Statistics of Two Indicators for Multilook Scattering Signals from Multilayered Structures with Slightly Rough Interfaces

Richard Dusséaux, Saddek Afifi

► **To cite this version:**

Richard Dusséaux, Saddek Afifi. Statistics of Two Indicators for Multilook Scattering Signals from Multilayered Structures with Slightly Rough Interfaces. Progress In Electromagnetics Research M, 2023, 115, pp.11-20. 10.2528/PIERM22092006 . hal-03938528

**HAL Id: hal-03938528**

**<https://hal.science/hal-03938528>**

Submitted on 13 Jan 2023

**HAL** is a multi-disciplinary open access archive for the deposit and dissemination of scientific research documents, whether they are published or not. The documents may come from teaching and research institutions in France or abroad, or from public or private research centers.

L'archive ouverte pluridisciplinaire **HAL**, est destinée au dépôt et à la diffusion de documents scientifiques de niveau recherche, publiés ou non, émanant des établissements d'enseignement et de recherche français ou étrangers, des laboratoires publics ou privés.

# Statistics of Two Indicators for Multilook Scattering Signals from Multilayered Structures with Slightly Rough Interfaces

Richard Dusséaux<sup>1, \*</sup> and Saddek Affi<sup>2</sup>

**Abstract**—Within the framework of the first-order small perturbation method, we derive the statistics of the layered rough surface index and the normalized difference polarization index for three-dimensional layered structures with slightly rough interfaces illuminated by a monochromatic plane wave and for multilook returns. We establish closed-form expressions for the probability density function and cumulative distribution function. The first- and second-order moments are given by relation recurrences. We validate from Monte Carlo simulations the obtained theoretical formulas.

## 1. INTRODUCTION

The co- and cross-polarized intensity ratios are useful indicators in the analysis of polarimetric and interferometric radar data [1–6]. In [4], we established the analytical expression of the probability density function (PDF) for the scattered intensity ratios for a three-dimensional layered structure with slightly rough interfaces illuminated by a monochromatic plane wave. The scattered intensities were obtained from the first-order small perturbation method (SPM) [7–12] with random interfaces having centered Gaussian height distributions. For single-look scattering intensities, we showed that the ratio obeyed heavy-tailed probability distribution, whose mean and variance are not defined.

It is important to define various combinations of polarized signatures to determine which combination is most suitable for land cover classification and characterization purposes. Some authors use normalized difference polarization index (NDPI) as an indicator. NDPI is defined as the ratio  $(I_{(ba)} - I_{(b'a')}) / (I_{(ba)} + I_{(b'a')})$  where the quantity  $I_{(ba)}$  designates the  $(b)$ -polarized component of the scattered intensity for the  $(a)$ -polarized incident wave. NDPI values extracted from polarimetric data are used for monitoring, analyzing, and labelling different land cover types [13, 14]. NDPI is a random variable defined over  $[-1; +1]$ , and contrary to the intensity ratio, the mean and variance values of this discriminator are finite. In [15], within the framework of the SPM, we determined the probability distribution of the NDPI, and for a sand layer covering a granite surface, we studied the combined influence of the interface anisotropy and their cross-correlation upon the probability laws. In [16], we defined the Layered Rough Surface Index (LRSI) to study stratified media. This indicator is defined as the ratio  $I_{(b'a')} / (I_{(ba)} + I_{(b'a')})$ . For a given observation direction, this descriptor is a random variable defined over  $[0; +1]$  and is characterized by a finite mean and a finite variance. For a structure air/clayey soil/rock, we analyzed the influence of a snow layer cover upon the distribution of the LRSI in the cases of Gaussian and exponential correlation functions, and we showed that the shape of the distribution was truly useful to differentiate the cases with and without snow cover.

Polarimetric signatures often exhibit substantial fluctuations, and it is often necessary to average data. Multilook return statistics were studied under the assumption of a multivariate Gaussian model

---

Received 20 September 2022, Accepted 24 November 2022, Scheduled 7 January 2023

\* Corresponding author: Richard Dusséaux (richard.dusseaux@latmos.ipsl.fr).

<sup>1</sup> Laboratoire Atmosphères, Milieux, Observations Spatiales (LATMOS), Université de Versailles Saint-Quentin-en-Yvelines (UVSQ/Paris-Saclay), 11 boulevard d'Alembert, Guyancourt 78280, France. <sup>2</sup> Electronics Department, Badji Mokhtar, Annaba University, BP 12, Annaba 23000, Algeria.

for the two underlying complex components of the field scattered by the random medium [1–3, 6]. The present paper is an extension of our previous works on the statistical properties of NDPI and LRSI in single-look [15, 16] and of the ratio of intensities in multi-looks [6]: we are interested in the statistical properties of the co- and cross-polarized LRSI and NDPI but for multilook configurations. We derive the theoretical expressions for the PDF and cumulative distribution function (CDF) for a stratified medium bounded by random slightly rough interfaces illuminated by a linearly polarized plane wave. Recurrence relations give access to the first- and second-order moments. To the best of the authors' knowledge, it is the first time that these analytical expressions are found.

## 2. THE MULTILOOK INTENSITY RATIO

The three-dimensional layered structure, analyzed here, is shown in Figure 1, which is composed of three non-magnetic regions characterized by an isotropic, homogeneous permittivity. The top and bottom regions are half-spaces. Relative permittivity values are  $\varepsilon_{r1} = 1$  for the top region that is assimilated to the vacuum,  $\varepsilon_{r2}$  for the layer, and  $\varepsilon_{r3}$  for the bottom region. The boundaries are denoted by  $z = a_1(x, y)$  and  $z = a_2(x, y) - u_0$  where both functions  $a_1(x, y)$  and  $a_2(x, y)$  are realizations of zero-mean stationary Gaussian random processes. The quantity  $u_0$  denotes the central layer thickness.

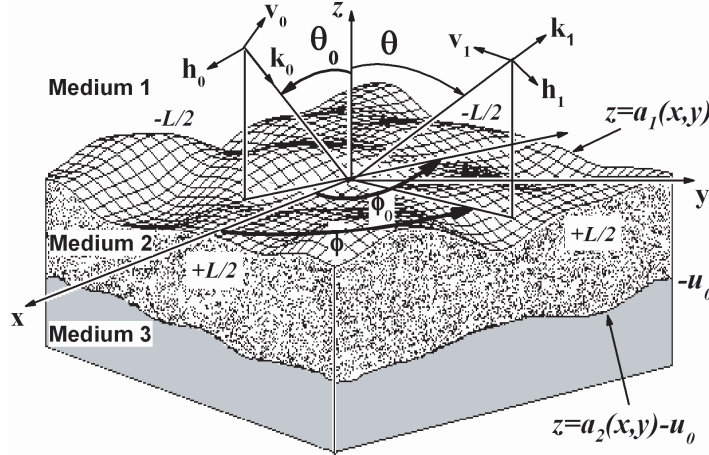


**Figure 1.** Structure with two nonparallel interfaces.

As shown in Figure 1, a monochromatic plane wave with wavelength  $\lambda$  is incident down onto the layered structure. The incident wave-vector direction is given by the zenith angle  $\theta_0$  and azimuth angle  $\phi_0$ . The incident plane wave gives rise after reflection to outgoing plane waves in all directions  $(\theta, \phi)$  of the upper region, whose first-order amplitudes are derived from the SPM as follows [7, 8]:

$$A_{1,(ba)}^{(1)}(\theta, \phi) = K_{1,(ba)}(\alpha, \beta) \hat{a}_1(\alpha - \alpha_0, \beta - \beta_0) + K_{2,(ba)}(\alpha, \beta) \hat{a}_2(\alpha - \alpha_0, \beta - \beta_0) \quad (1)$$

with  $\alpha = k \sin \theta \cos \phi$ ,  $\beta = k \sin \theta \sin \phi$ ,  $\alpha_0 = k \sin \theta_0 \cos \phi_0$ ,  $\beta_0 = k \sin \theta_0 \sin \phi_0$ , and  $k = 2\pi/\lambda$ . The subscript  $(a)$  gives the incident plane wave polarization (horizontal or vertical) and the subscript  $(b)$ , that of the scattered wave ( $h$  or  $v$ ), respectively. The function  $\hat{a}_i(\alpha, \beta)$  is the 2D Fourier transform of  $a_i(x, y)$ . The complex coefficients  $K_{i,(ba)}(\alpha, \beta)$  designate the first-order SPM kernels [7–12]. We recall that the first-order SPM is a low frequency approach valid for small roughness, and the surface height function must satisfy two restrictions: First, the root-mean-square height of the rough interface is small compared to the incident wavelength, and secondly, the gradient of the interface is small in comparison to unity [17, 18].

Within the framework of the SPM, the ratio between the scattered intensities  $I_{(ba)}(\theta, \phi)$  and

$I_{(b'a')}(\theta, \phi)$  is defined by

$$V_{(ba,b'a')}(\theta, \phi) = \frac{|A_{(ba)}^{(1)}(\theta, \phi)|^2}{|A_{(b'a')}^{(1)}(\theta, \phi)|^2} \quad (2)$$

The intensity ratio  $V_{(ba,b'a')}(\theta, \phi)$  depends on rough boundary height profile realizations, and for a given direction, it is a random variable.

Any linear operator transforms a Gaussian process into another Gaussian process. Since the height distributions of each rough interface are Gaussian, and the Fourier transform is a linear operation, we deduce that the joint PDF of the real and imaginary parts of the complex scattered amplitudes  $A_{(ba)}^{(1)}(\theta, \phi)$  and  $A_{(b'a')}^{(1)}(\theta, \phi)$  is a 4D-Gaussian function. In [4], the PDF  $p_{V_{(ba,b'a')}}(v)$  of the intensity ratio  $V_{(ba,b'a')}(\theta, \phi)$  was derived from this joint distribution, and a heavy-tailed distribution was obtained

$$p_{V_{(ba,b'a')}}(v) = \frac{(1 - r^2)p_0(v + p_0)}{[v^2 + 2vp_0(1 - 2r^2) + p_0^2]^{3/2}} \quad (3)$$

where  $v \geq 0$ . The first- and second-order moments of the random variable  $V_{(ba,b'a')}(\theta, \phi)$  are infinite. The two parameters of  $p_{V_{(ba,b'a')}}(v)$  are the modulus  $r$  of the complex correlation coefficient between the scattered amplitudes  $A_{(ba)}^{(1)}(\theta, \phi)$  and  $A_{(b'a')}^{(1)}(\theta, \phi)$  and the ratio  $p_0$  between the associated average intensities. In [4], we showed that the parameters  $r$  and  $p_0$  are functions of the first-order SPM kernels, on the spectrum of each interface and their cross-spectrum, and on the incidence and observation angles.

The  $n$ -look intensities are defined as follows:

$$\bar{I}_{n,(ba)}(\theta, \phi) = \frac{1}{n} \sum_{i=1}^n I_{(ba),i}(\theta, \phi) \quad (4)$$

In [6], we obtained a 3-parameter probability distribution for the  $n$ -look intensity ratio  $V_{n,(ba,b'a')} = \bar{I}_{n,(ba)}/\bar{I}_{n,(b'a')}$ ,

$$p_{V_{n,(ba,b'a')}}(v) = \frac{\Gamma(2n)}{\Gamma(n)\Gamma(n)} \frac{(1 - r^2)^n p_0^n v^{n-1} (v + p_0)}{[v^2 + 2vp_0(1 - 2r^2) + p_0^2]^{n+1/2}} \quad (5)$$

where the letter  $\Gamma$  designates the Gamma function. In [6], we also established the analytical expression for the CDF

$$F_{V_{n,(ba,b'a')}}(v) = F_{V_{1,(ba,b'a')}}(v) + \frac{v - p_0}{\sqrt{v^2 + 2vp_0(1 - 2r^2) + p_0^2}} \times \sum_{m=1}^{n-1} \frac{\Gamma(2m)}{m\Gamma(m)\Gamma(m)} \left[ \frac{(1 - r^2)p_0 v}{v^2 + 2vp_0(1 - 2r^2) + p_0^2} \right]^m \quad (6)$$

where the function  $F_{V_{1,(ba,b'a')}}(v)$  is the CDF for a single-look intensity ratio,

$$F_{V_{1,(ba,b'a')}}(v) = \frac{1}{2} + \frac{v - p_0}{2\sqrt{v^2 + 2vp_0(1 - 2r^2) + p_0^2}}. \quad (7)$$

We deduce from (6) and (7) that the parameter  $p_0$  is the median of the  $n$ -look intensity ratio for any value of  $n$ , and in [6], we showed that the mean  $m_{V_n}$  exists for  $n > 1$  and the variance  $\sigma_{V_{n,(ba,b'a')}}^2$  for  $n > 2$ , respectively:

$$m_{V_n} = \frac{(n - r^2)p_0}{(n - 1)} \quad (8)$$

$$\sigma_{V_n}^2 = \frac{p_0^2}{(n - 1)^2(n - 2)} \{n(2n - 1) - r^2 [4(n - 1)(1 - r^2) + n(2n - r^2)]\}. \quad (9)$$

### 3. STATISTICS OF THE MULTILOOK LRSI

Let  $S_{n,(b'a',ba)} = \bar{I}_{n,(b'a')}/(\bar{I}_{n,(ba)} + \bar{I}_{n,(b'a')})$  be the multilook LRSI associated with the components  $(b'a')$  and  $(ba)$  of the wave scattered in the direction  $(\theta, \phi)$ . Knowing that  $S_{n,(b'a',ba)} = 1/(V_{n,(ba,b'a')} + 1)$ , the PDF of  $S_{n,(b'a',ba)}$  is determined from the following transformation,

$$p_{S_{n,(b'a',ba)}}(s) = \left| \frac{dv(s)}{ds} \right| p_{V_{n,(ba,b'a')}}[v(s)] = \frac{1}{s^2} p_{V_{n,(ba,b'a')}}[v(s)] \quad (10)$$

where  $v = (1 - s)/s$ , and we obtain the PDF defined on  $[0; 1]$ ,

$$p_{S_{n,(b'a',ba)}}(s) = \frac{\Gamma(2n) p_0^n (1 - r^2)^n (s - s^2)^{n-1} [s(p_0 - 1) + 1]}{\Gamma^2(n) R_S^{n+1/2}} \quad (11)$$

with

$$R_S = s^2 [(1 - p_0)^2 + 4r^2 p_0] + 2s [(p_0 - 1) - 2r^2 p_0] + 1. \quad (12)$$

The CDF of the continuous random variable  $S_{n,(b'a',ba)}$  is the primitive function of its PDF. After some mathematical manipulations, we obtain

$$F_{S_{n,(ba,b'a')}}(s) = 1 - F_{V_{n,(ba,b'a')}}\left(\frac{1-s}{s}\right). \quad (13)$$

Finally, by substituting (7) into (13), we show that the CDF of the multilook LRSI is defined as follows:

$$F_{S_{n,(ba,b'a')}}(s) = F_{S_{1,(ba,b'a')}}(s) + \frac{s(1+p_0) - 1}{R_S^{1/2}} \sum_{m=1}^{n-1} \frac{\Gamma(2m)}{m\Gamma(m)\Gamma(m)} \left( \frac{(1-r^2)p_0 s (1-s)}{R_S} \right)^m. \quad (14)$$

The function  $F_{S_{1,(ba,b'a')}}(s)$  is the CDF for a single-look LRSI. We established in [16] that

$$F_{S_{1,(ba,b'a')}}(s) = \frac{1}{2} + \frac{s(p_0 + 1) - 1}{2R_S^{1/2}}. \quad (15)$$

We deduce from (14) and (15) that the median of the multilook LRSI is  $1/(1+p_0)$  and does not depend on the number of looks.

We derive from (11) a recurrence relation for  $p_{S_{n,(ba,b'a')}}(s)$  and  $p_{S_{n+1,(ba,b'a')}}(s)$ :

$$\begin{aligned} & \{s^2 [(p_0 - 1)^2 + 4r^2 p_0] + 2s(p_0 - 1 - 2r^2 p_0) + 1\} p_{S_{n+1,(ba,b'a')}}(s) \\ &= \frac{2(2n+1)}{n} p_0 (1 - r^2) s (1 - s) p_{S_{n,(ba,b'a')}}(s). \end{aligned} \quad (16)$$

By integrating the recurrence relation from 0 to 1, we obtain a recurrence relation for the means  $m_{S_n}$  and  $m_{S_{n+1}}$ :

$$[(p_0 - 1)^2 + 4r^2 p_0] m_{S_{n+1}} + 2(p_0 - 1 - 2r^2 p_0) + \int_0^1 \frac{p_{S_{n+1,(ba,b'a')}}(s)}{s} ds = \frac{2(2n+1)}{n} p_0 (1 - r^2) (1 - m_{S_n}). \quad (17)$$

Using the change of variable  $s = 1/(v + 1)$ , we show that

$$\int_0^1 \frac{p_{S_{n+1,(ba,b'a')}}(s)}{s} ds = \int_0^{+\infty} v p_{V_{n+1,(ba,b'a')}}(v) dv + 1 = 1 + m_{V_{n+1}}. \quad (18)$$

By substituting (8) and (18) into (17), we obtain the first-order moment for the multilook LRSI by the following recurrence relation:

$$m_{S_{n+1}} = \frac{(1+p_0)n + (1-r^2)p_0 - 2(2n+1)p_0(1-r^2)m_{S_n}}{[(p_0 - 1)^2 + 4r^2 p_0] n}. \quad (19)$$

In [16], we established the analytical expression of the mean  $m_{S_1}$  for a single-look LRSI with

$$m_{S_1} = \frac{2p_0r^2 - (p_0 - 1)}{(p_0 - 1)^2 + 4p_0r^2} + \frac{p_0(p_0 - 1)(1 - r^2)}{[(p_0 - 1)^2 + 4p_0r^2]^{3/2}} \ln \left( p_0 \frac{\sqrt{(p_0 - 1)^2 + 4p_0r^2} + (p_0 - 1) + 2r^2}{\sqrt{(p_0 - 1)^2 + 4p_0r^2} + (p_0 - 1) - 2p_0r^2} \right). \quad (20)$$

We also find from (17) a four-term recurrence relation for the first- and second-order moments  $m_{S_n}$ ,  $m_{S_{n+1}}$ ,  $m_{S_n^2}$  and  $m_{S_{n+1}^2}$ :

$$[(p_0 - 1)^2 + 4r^2p_0] m_{S_{n+1}^2} = -2(p_0 - 1 - 2r^2p_0)m_{S_{n+1}} + 1 + \frac{2(2n + 1)}{n}p_0(1 - r^2)(m_{S_n} - m_{S_n^2}). \quad (21)$$

The first-term  $m_{S_1^2}$  of this recurrence relation was established in [16] with

$$m_{S_1^2} = \frac{(p_0 + 1) [(p_0 - 1)^2 + p_0r^2(3 - p_0)] - 8p_0^2r^2(1 - r^2)}{[(p_0 - 1)^2 + 4p_0r^2]^2} + \frac{2p_0(1 - r^2) [p_0r^2(3p_0 - 1) - (p_0 - 1)^2]}{[(p_0 - 1)^2 + 4p_0r^2]^{5/2}} \ln \left[ p_0 \frac{\sqrt{(p_0 - 1)^2 + 4p_0r^2} + (p_0 - 1) + 2r^2}{\sqrt{(p_0 - 1)^2 + 4p_0r^2} + (p_0 - 1) - 2p_0r^2} \right]. \quad (22)$$

We show from (19) that  $\lim_{n \rightarrow \infty} m_{S_n} = 1/(1 + p_0)$  and from (21) that  $\lim_{n \rightarrow \infty} m_{S_n^2} = m_{S_n^2}^*$ . As a result, the variance  $\sigma_{S_n}^2 = m_{S_n^2} - m_{S_n}^2$  tends asymptotically toward zero. The random variable  $S_{n,(b'a',ba)}$  is almost surely a constant. It always has the same value  $1/(1 + p_0)$  that is the median.

#### 4. STATISTICS OF THE MULTILOOK NDPI

The multilook NDPI  $W_{n,(ba,b'a')}$  is defined as  $W_{n,(ba,b'a')} = (\bar{I}_{n,(ba)} - \bar{I}_{n,(b'a')})/(\bar{I}_{n,(ba)} + \bar{I}_{n,(b'a')})$  and takes values in  $[-1; +1]$ . We determine its PDF from the following transformation

$$pW_{n,(ba,b'a')}(w) = \left| \frac{ds(w)}{dw} \right| pS_{n,(ba,b'a')}(s(w)) \quad (23)$$

where  $s = (1 - w)/2$ . For  $-1 \leq w \leq +1$ , we find that

$$PW_{n,(ba,b'a')}(w) = \frac{2\Gamma(2n)}{\Gamma(n)\Gamma(n)} \frac{(1 - r^2)^n p_0^n (1 - w^2)^{n-1} [w(1 - p_0) + (1 + p_0)]}{R_W^{n+1/2}} \quad (24)$$

with

$$R_W = w^2 [(1 - p_0)^2 + 4r^2p_0] + 2w(1 - p_0^2) + (1 + p_0)^2 - 4r^2p_0. \quad (25)$$

The CDF of  $W_{n,(ba,b'a')}$  is obtained by the integral of its PDF. After some mathematical manipulations, we obtain

$$FW_{n,(ba,b'a')}(w) = 1 - F_{S_{n,(ba,b'a')}} \left( \frac{1 - w}{2} \right). \quad (26)$$

Finally, substituting (14) into (26), we obtain the CDF of the multilook NDPI as follows:

$$FW_{n,(ba,b'a')}(w) = FW_{1,(ba,b'a')}(w) + \frac{w(1 + p_0) + 1 - p_0}{R_W^{1/2}} \sum_{m=1}^{n-1} \frac{\Gamma(2m)}{m\Gamma(m)\Gamma(m)} \left( \frac{(1 - r^2)p_0(1 - w^2)}{R_W} \right)^m. \quad (27)$$

The function  $FW_{1,(ba,b'a')}(w)$  is the CDF for a single-look NDPI. We established in [15] that

$$FW_{1,(ba,b'a')}(w) = \frac{1}{2} + \frac{w(1 + p_0) + 1 - p_0}{2R_W^{1/2}}. \quad (28)$$

We deduce from (27) and (28) that the median of the  $n$ -look NDPI is  $(p_0 - 1)/(p_0 + 1)$ . Knowing that  $W_{n,(ba,b'a')} = 1 - 2S_{n,(ba,b'a')}$ , we deduce the first- and second-order moments of  $W_{n,(ba,b'a')}$

$$m_{W_n} = 1 - 2m_{S_n}. \quad (29)$$

$$m_{W_n^2} = 4m_{S_n^2} - 4m_{S_n} + 1. \quad (30)$$

We show that  $\lim_{n \rightarrow \infty} m_{W_n} = (p_0 - 1)/(p_0 + 1)$  and  $\lim_{n \rightarrow \infty} m_{W_n^2} = m_{W_n}^2$ . As a result, the variance  $\sigma_{W_n}^2$  tends asymptotically toward zero. The random variable  $W_{n,(b'a',ba)}$  is almost surely a constant. It always has the same value  $(p_0 - 1)/(p_0 + 1)$  that is the median.

The closed form expressions of the probability density function and the cumulative density function for the LRSI and the NDPI and the recurrence relations giving the first- and second-order moments are valid whatever the value of the number of looks. Nevertheless, we have to keep in mind that these expressions are valid under the assumption of a multivariate Gaussian model for the real and imaginary parts of the two underlying components of the field scattered by the illuminated zone.

## 5. THEORETICAL AND NUMERICAL RESULTS

Consider a stack of two rough surfaces illuminated by a monochromatic plane wave of wavelength  $\lambda$  equal to 24 cm. The relative permittivity values are  $\varepsilon_{r2} = 4.66 - 0.29j$  and  $\varepsilon_{r3} = 8.75 - 0.85j$ . The Gaussian spectrum of the first random interface is anisotropic with the Ox-correlation length equal to 5 cm and the Oy-correlation length equal to 4 cm [6]. The Gaussian spectrum of the second interface is isotropic with a correlation length equal to 6 cm. The correlation coefficient between the two rough interfaces is equal to 1/5. The root-mean-square heights are equal to 0.5 cm and 0.4 cm, respectively. The average thickness  $u_0$  of the central layer is equal to 5 cm. The zenith angle  $\theta_0$  and azimuth angle  $\phi_0$  of the incident wave vector are equal to  $30^\circ$  and  $0^\circ$ , respectively. The values chosen for the rms-heights and the correlation lengths allow the use of the first-order SPM and correspond to certain slightly rough agricultural soils [19–21]. These values can correspond approximatively to soil moistures in volumetric content of 10% and 20% [22].

Figure 2 shows the PDF of the LRSI  $S_{n,(hh,vv)}$  in the backscattering direction for  $n = 1, 2, 4,$  and  $8$ . The theoretical PDFs are given by (11) and assume surfaces of infinite extent. The histograms in Figure 2 are obtained from Monte-Carlo simulations considering a set of  $2^{13}$  stratified structures with  $L = 20\lambda$  and the associated scattered amplitudes given by (1). Figure 3 shows the theoretical CDF curves obtained from (14) and those obtained by Monte-Carlo simulations. The height profile functions are generated by Gaussian filters applied to uncorrelated white Gaussian noise realizations. The generation process of correlated interfaces is described in [16]. The Fourier Transform in Eq. (1) is calculated by fast Fourier transform (FFT). The first-order SPM kernels are given in [6, 7]. Comparison is conclusive for each value of  $n$ . Such comparisons were made for the  $n$ -look NDPI and for observation

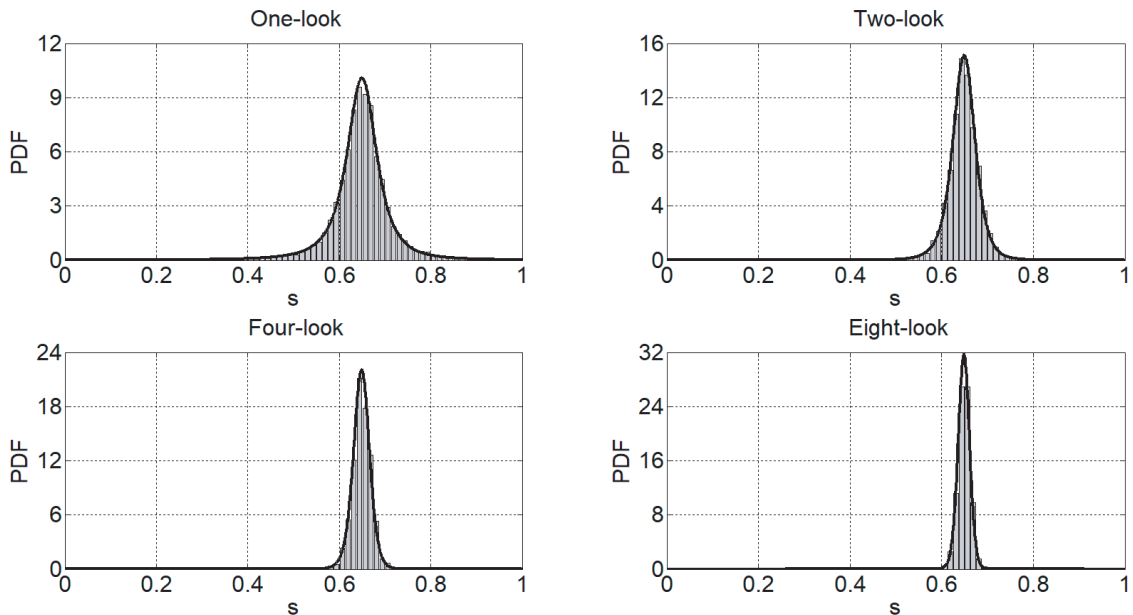


**Figure 2.** PDF of the  $n$ -look LRSI  $S_{n,(hh,vv)}$  for  $n = 1, 2, 4$  and  $8$ .

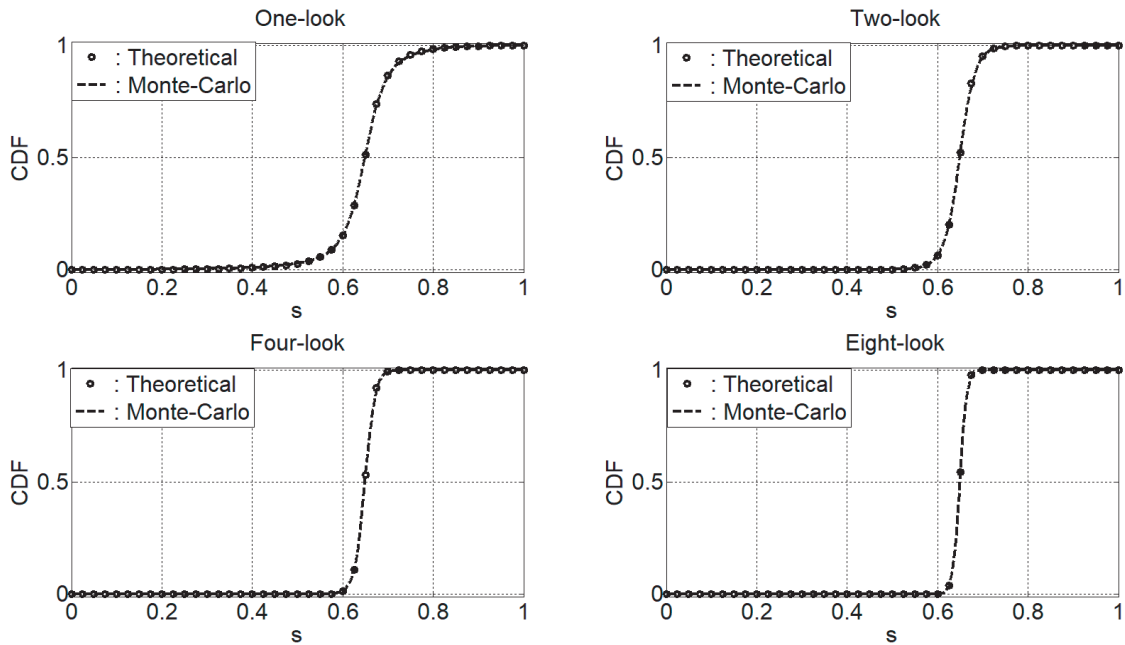


**Figure 3.** CDF of the  $n$ -look LRSI  $S_{n,(hh,vv)}$  for  $n = 1, 2, 4$  and  $8$ .

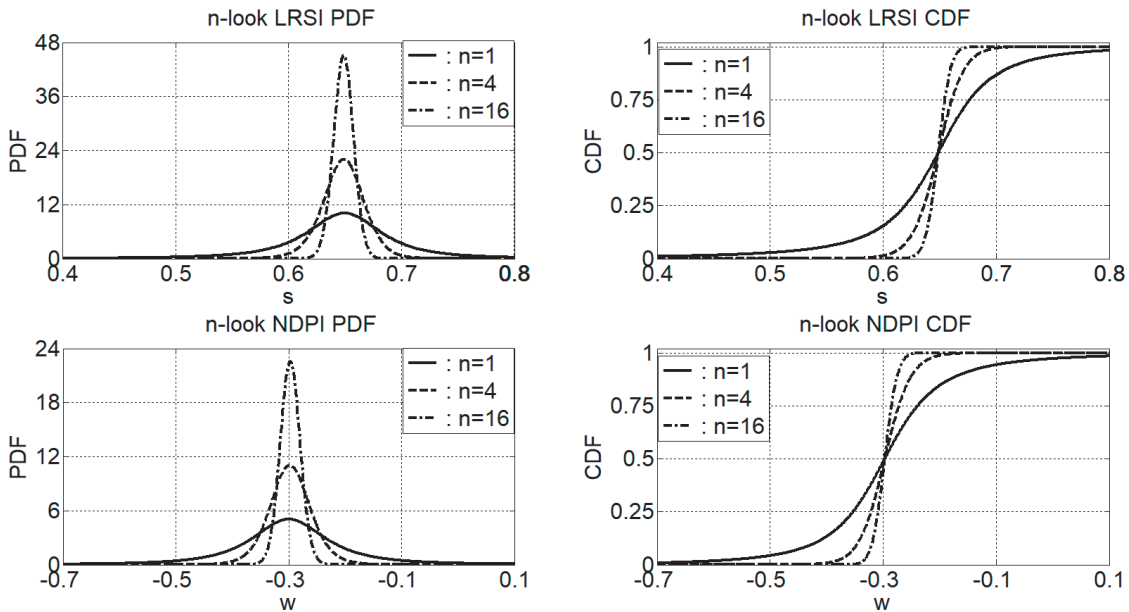


**Figure 4.** PDF and CDF of  $S_{n,(hh,vv)}$  and  $W_{n,(hh,vv)}$  for  $n = 1, 4$  and  $16$ .

directions outside the incidence plane considering the co- and cross-polarized  $n$ -look LRSI and NDPI. Comparisons were also conclusive but not shown here.

Figure 4 shows the PDF and CDF of  $S_{n,(hh,vv)}$  and  $W_{n,(hh,vv)}$  in the backscattering direction for  $n = 1, 4$ , and  $16$ . The multi-look processing reduces the statistical fluctuations, and the standard deviations decrease when  $n$  increases. Consequently, the width of the NDPI- and LRSI-PDF curves decreases when the number of looks increases, and the maximum value increases. The PDF of  $S_{n,(hh,vv)}$  is defined on the interval  $[0; 1]$  and that of  $W_{n,(hh,vv)}$  on the interval  $[-1; 1]$ . We can note that the

maximum value of the PDF of  $S_{n,(hh,vv)}$  is about twice that of the PDF of  $W_{n,(hh,vv)}$ . Given the electrical and geometrical parameter values,  $p_0 = 0.5418$ . The median for the LRSI is equal to 0.6486 and for the NDPI, to 0.2972, respectively. The CDF curves intersect at the same point showing that the median does not depend on the number of looks. As the number of looks increases, the CDF becomes identified with a Heaviside function shifted on the median value equal to  $(p_0 - 1)/(p_0 + 1)$  for the NDPI and to  $1/(p_0 + 1)$  for the LRSI, respectively, and the PDFs converge to Dirac Delta distributions shifted on the median values. As shown in Figures 2 and 3, this behavior is well reproduced by Monte Carlo simulations. For a surface separating two homogeneous media, the (hh)-backscattered intensity is lower than the (vv)-intensity [4]. For a stack of two random interfaces, the probability of the event  $\{I_{hh} > I_{vv}\}$  has a non-zero probability in the backscatter direction. The probability of the event  $\{I_{hh} > I_{vv}\}$  becomes identified with  $1 - F_{W_{1,(hh,vv)}}(0)$  or with  $F_{S_{1,(vv, hh)}}(0.5)$ . This probability is equal to 0.0280. This means that the (hh)-intensity is greater than the (vv)-intensity for only 2.8% of the realizations of the stratified medium (236 cases observed out of  $2^{13}$  simulated). In a similar way, we can determine the probability of the event  $\{\bar{I}_{n, hh} > \bar{I}_{n, vv}\}$ . We find:  $\Pr\{\bar{I}_{2, hh} > \bar{I}_{2, vv}\} = 0.23 \times 10^{-2}$ ,  $\Pr\{\bar{I}_{4, hh} > \bar{I}_{4, vv}\} = 0.20 \times 10^{-4}$  and  $\Pr\{\bar{I}_{16, hh} > \bar{I}_{16, vv}\} < 10^{-15}$ . The event  $\{\bar{I}_{n, hh} > \bar{I}_{n, vv}\}$  becomes asymptotically a null-event and has no outcomes, and we find the result obtained in backscattering for a single surface separating two homogeneous media.

Figure 5 shows the mean and standard deviation of the random variables  $S_{n,(hh,vv)}$  and  $W_{n,(hh,vv)}$  as a function of  $n$ . These theoretical values are compared with those obtained from the set of realizations. The comparison is conclusive. Nevertheless, curves show very small differences between theoretical values and simulation results. Given the simulation parameter values, the theoretical value of the modulus  $r$  of the correlation coefficient between the scattered amplitudes  $A_{1,(hh)}^{(1)}$  and  $A_{1,(vv)}^{(1)}$  is equal to 0.9941, and the ratio  $p_0$  is equal to 0.5418. The theory assumes surfaces with infinite extent. Values obtained from the set of  $2^{13}$  scattered amplitudes associated with the set of  $2^{13}$  realizations of the sub-surfaces with  $L = 20\lambda$  are equal to 0.9938 and 0.5403, respectively. It should be kept in mind that the differences between the theoretical values of  $r$  and  $p_0$  and the values obtained from Monte-Carlo simulations as well as the shifts observed on the curves decrease when the size of the generated surfaces increases. It can be noticed that whatever the number of looks, the means are close to the asymptotic values which correspond to the medians and that the standard deviations decrease when the number of looks increases, and they are less than 1% of the PDF support from  $n \geq 14$ .

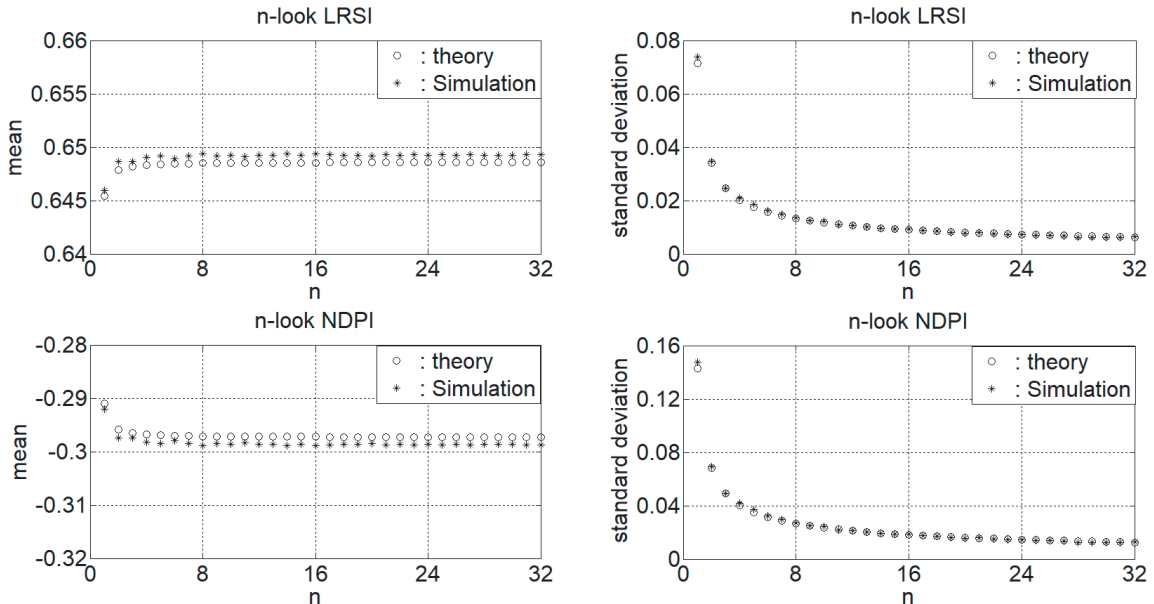


**Figure 5.** Mean and standard deviation versus number of looks for the  $n$ -look LRSI  $S_{n,(hh,vv)}$  and for the  $n$ -look NDPI  $W_{n,(hh,vv)}$ .

## 6. CONCLUSION

Within the framework of the first-order SPM, we have established the theoretical statistics of two indicators, the LRSI and NDPI, for multilook signals scattered from multi-layered structures with slightly rough interfaces under an illumination by a monochromatic plane wave. The closed-form expressions for the PDFs and CDFs were obtained, and recurrence relations give access to the first- and second-order moments.

For a two-layer rough ground, we have verified the effectiveness of the theory by comparing it with the Monte Carlo simulation results. It should be kept in mind that whatever the random medium studied, if the real and imaginary parts of the field scattered by the illuminated zone are Gaussian random processes, the analytical expressions obtained for the  $n$ -look LRSI and  $n$ -look NDPI can be used.

Nevertheless, the roughness of some natural or agricultural surfaces does not obey a Gaussian height distribution. For example, the height distribution of some ploughed soils is not Gaussian [23, 24]. For non-Gaussian slightly rough surfaces, we do not know how to conclude on the nature of the joint distribution of the real and imaginary parts of the scattering amplitudes. The use of the central limit theorem deserves to be justified [25, 26]. It therefore appears useful to derive the analytical expression for the joint probability distribution of the real and imaginary parts of the two underlying complex scattering amplitudes within the framework of the small perturbation method. Moreover, the use of an exact method or another analytical method seems unavoidable if the interfaces of the stratified medium are strongly or moderately rough [11, 22, 27]. For Gaussian and non-Gaussian surfaces with a moderate or high roughness, the first-order small perturbation method cannot be used, and the statistics for the LRSI and the NDPI, in both single-look and multi-looks cases, remain established, either by an analytical approach or by Monte-Carlo simulations. This is an open question that requires work in its own right.

## REFERENCES

1. Kong, J. A., A. A. Swartz, H. A. Yueh, L. M. Novak, and R. T. Shin, "Identification of terrain cover using the optimum polarimetric classifier," *Journal of Electromagnetic Waves and Applications*, Vol. 8, No. 2, 171–194, 1988.
2. Lee, J. S., K. W. Hoppel, S. A. Mango, and A. R. Miller, "Intensity and phase statistics of multilook polarimetric and interferometric SAR imagery," *IEEE Trans. Geosci. Remote Sensing*, Vol. 32, No. 5, 1017–1028, Sep. 1994.
3. Joughin, I. R., D. P. Winebrenner, and D. B. Percival, "Probability density functions for multilook polarimetric signatures," *IEEE Trans. Geosci. Remote Sens.*, Vol. 32, No. 3, 562–574, May 1994.
4. Affi, S. and R. Dusséaux, "On the co-polarized scattered intensity ratio of rough layered surfaces: The probability law derived from the small perturbation method," *IEEE Trans. Antennas Propag.*, Vol. 60, No. 4, 2133–2138, Apr. 2012.
5. Affi, S. and R. Dusséaux, "The co- and cross-polarized scattered intensity ratios for 3D layered structures with randomly rough interfaces," *Journal of Electromagnetic Waves and Applications*, Vol. 33, No. 7, 811–826, 2019.
6. Dusséaux, R. and S. Affi, "Multilook intensity ratio distribution for 3D-layered structures with slightly rough interfaces," *IEEE Trans. Antennas Propag.*, Vol. 68, No. 7, 5575–5582, Jun. 2020.
7. Tabatabaenejad, A. and M. Moghaddam, "Bistatic scattering from three-dimensional layered rough surfaces," *IEEE Trans. Geosci. Remote Sens.*, Vol. 44, No. 8, 2102–2114, Aug. 2006.
8. Imperatore, P., A. Iodice, and D. Riccio, "Electromagnetic wave scattering from layered structures with an arbitrary number of rough interfaces," *IEEE Trans. Geosci. Remote Sens.*, Vol. 47, No. 4, 1056–1072, Apr. 2009.
9. Lin, Z. W., X. J. Zhang, and G. Y. Fang, "Theoretical model of electromagnetic scattering from 3D multi-layer dielectric media with slightly rough surfaces," *Progress In Electromagnetics Research*, Vol. 96, 37–62, 2009.

10. Berrouk, A., R. Dusséaux, and S. Affi, “Electromagnetic wave scattering from rough layered interfaces: Analysis with the small perturbation method and the small slope approximation,” *Progress In Electromagnetics Research B*, Vol. 57, 177–190, 2014.
11. Affi, S., R. Dusséaux, and A. Berrouk, “Electromagnetic wave scattering from 3D layered structures with randomly rough interfaces: Analysis with the small perturbation method and the small slope approximation,” *IEEE Trans. Antennas Propagat.*, Vol. 62, No. 10, 5200–5208, Oct. 2014.
12. Djedouani, N., S. Affi, and R. Dusséaux, “Inversion of electrical and geometrical parameters of a stratified medium from data derived from the Small Perturbation Method and the Small Slope Approximation,” *Progress In Electromagnetics Research B*, Vol. 94, 19–36, 2021.
13. Mishra, P. and D. Singh, “Role of polarimetric indices based on statistical measures to identify various land cover classes in ALOS PALSAR data,” *Proc. APSAR*, 1–4, Seoul, South Korea, Sep. 2011.
14. Mishra, P. and D. Singh, “A statistical-measure-based adaptive land cover classification algorithm by efficient utilization of polarimetric SAR observables,” *IEEE Trans. Geosc. Remote Sens.*, Vol. 52, No. 5, 2889–2900, Oct. 2014.
15. Affi, S. and R. Dusséaux, “Statistical distribution of the Normalized Difference Polarization Index for 3D layered structures with slightly rough interfaces,” *IEEE Trans. Antennas Propag.*, Vol. 67, No. 6, 4291–4295, Jun. 2019.
16. Dusséaux, R. and S. Affi, “Statistical distribution of the Layered Rough Surface Index (LRSI),” *Progress In Electromagnetics Research C*, Vol. 94, 75–87, 2019.
17. Elfouhaily, T. M. and C. A. Guérin, “A critical survey of approximate scattering wave theories from random rough surfaces,” *Waves Random Media*, Vol. 14, R1–R40, 2004.
18. Tabatabaenejad, A. and M. Moghaddam, “Study of validity region of small perturbation method for two-layer rough surfaces,” *IEEE Geosci. Remote Sens. Lett.*, Vol. 7, No. 2, 319–323, Feb. 2010.
19. Zribi, M., O. Taconet, S. Le Hégarat-Masclé, D. Vidal-Madjar, C. Emblanch, C. Loumagne, and M. Normand, “Backscattering behavior and simulation comparison over bare soils using SIR-C/X-SAR and ERASME 1994 data over Orgeval,” *Remote Sens. Env.*, Vol. 59, No. 2, 256–266, 1997.
20. Boisvert, J. B., Q. H. J. Gwyn, A. Chanzy, D. J. Major, B. Brisco, and R. J. Brown, “Effect of surface soil moisture gradients on modelling radar backscattering from bare fields,” *Int. J. Remote Sens.*, Vol. 18, No. 1, 153–170, 1997.
21. Zribi, M., M. Sahnoun, N. Baghdad, T. Le Toan, and A. Ben Hamida, “Analysis of the relationship between backscattered P-band radar signals and soil roughness,” *Remote Sens. Env.*, Vol. 181, 13–21, 2016.
22. Tsang, L., J. A. Kong, K. H. Ding, and C. O. Ao, *Scattering of Electromagnetic Waves — Numerical Simulations*, Wiley, New-York, 2001.
23. Dusséaux, R., E. Vannier, O. Taconet, and G. Granet, “Study of backscatter signature for seedbed surface evolution under rainfall — Influence of radar precision,” *Progress In Electromagnetics Research*, Vol. 125, 415–437, 2012.
24. Vannier, E., O. Taconet, R. Dusséaux, and O. C. Chiadjeu, “Statistical characterization of bare soil surface microrelief,” *Adv. Geosci. Remote Sens.*, 207–228, 2014.
25. Abdi, A., H. Hashemi, and S. Nader-Esfahani, “On the PDF of the sum of random vectors,” *IEEE Trans. Commun.*, Vol. 48, No. 1, 7–12, Jan. 2000.
26. Jakeman, E. and K. D. Ridley, *Modeling Fluctuations in Scattered Waves*, Taylor and Francis, New York, 2006.
27. Bourlier, C., N. Pinel, and G. Kubické, *Method of Moments for 2D Scattering Problems: Basic Concepts and Applications*, Wiley, Hoboken, NJ, USA, 2013.